Kinetics of hydrogen-evolution reaction on lead and lead-alloy electrodes in sulfuric acid electrolyte with phosphoric acid and antimony additives

S. Venugopalan
Batteries Division, Power Systems Group, ISRO Satellite Centre, Bangalore-560017 (India)

(Received July 13, 1993; accepted October 29, 1993)

Abstract

The kinetics of the hydrogen-evolution reaction (HER) on smooth Pb, Pb–Ca–Sn and Pb–Sb–Se alloy electrodes is studied in H_2SO_4 (3–10 M) electrolyte that contains phosphoric acid (0–40 g l^{-1}) and antimony (0–10 mg l^{-1}) using galvanostatic polarization in the Tafel domain. A direct correlation is found between $i_{0,H}$ and i_{cor} on lead and lead-alloy electrodes with varying concentrations of H_3PO_4 and Sb(III) in H_2SO_4. The maximum suppression of the HER occurs with 20 g l^{-1} H_3PO_4 in H_2SO_4 for both lead and lead alloys. The data are explained in the light of a model that employs adsorption of H_3PO_4 at the electrode/electrolyte interface.

Introduction

It has been documented in the literature that incorporation of antimony either in the positive active material [1] or in the grid material [2, 3] improves the deep-discharge cycle life of the lead/acid cell. Antimony is known, however, to leach out into the electrolyte [4] and cause deleterious effects on the performance of the lead electrode. Sealed lead/acid (SLA) cells, therefore, employ Pb–Ca alloys as grid materials in order to suppress the HER. This causes the 'antimony-free effect' [5]. To counter this effect in SLA cells additives such as H_3PO_4 have been employed [6]. But studies of their role on the kinetics of the HER have been largely neglected. The only previous investigation is that of Song and Chen [7]. This is because most of the studies [8–10] have employed fast sweep techniques, such as cyclic and linear sweep voltammetry, that exhibit non-steady-state behaviour. Also, there is little information on the overall effect of antimony in the presence of H_3PO_4 in the H_2SO_4 electrolyte.

In this study, therefore, the effects of phosphoric acid and antimony additives in the sulfuric acid electrolyte on the kinetics of the HER on lead and lead-alloy grid materials has been examined by a steady-state polarization technique in the Tafel and linear domains. The study suggests that the deleterious effects of antimony are inhibited in the presence of phosphoric acid in the electrolyte.

Experimental

The technique, apparatus, experimental conditions and procedure were identical to those described previously [11].

SSDI 0378-7753(93)01881-H

Results and discussion

In the case of lead and lead alloys, hydrogen evolution is the only cathodic conjugate reaction of corrosion in de-oxygenated sulfuric acid. The corrosion of lead is thus related to the kinetics of the cathodic hydrogen-evolution reaction and the anodic metal dissolution reaction. At the corrosion potential (steady-state open-circuit potential), in solutions depleted of Pb^{2+} ions, the electrode reactions to be considered are:

$$Pb \longrightarrow Pb^{2+} + 2e^- \quad (1)$$

$$2H^+ + 2e^- \longrightarrow H_2 \quad (2)$$

Reactions (1) and (2) are occurring under totally irreversible conditions, i.e., $(E - E_{cor}) = \xi^* \gg RT/F$. Under these irreversible conditions, the steady-state current–potential relation under cathodic Tafel conditions may be expressed as:

$$\frac{i}{i_{cor}} = \exp[-\alpha_H f(E - E_{cor})] \quad (3)$$

or,

$$\xi = \frac{1}{\alpha_H f} \ln i_{cor} - \frac{1}{\alpha_H f} \ln i \quad (4)$$

where the symbols have their meaning as explained under the supplied list of symbols.

The validity of the above assumptions underlying the Tafel behaviour (E versus log i as a straight line) was easily verified with the experimental data obtained in this study since, in practically all the cases, well-defined, reproducible, steady-state, hysteresis-free Tafel plots were obtained over two decades or more of the current density. It is claimed that this is the first time that experimental conditions have been standardized rigorously to get highly reproducible hysteresis-free Tafel plots for the HER on lead and lead alloys in sulfuric acid solutions.

A comparison of the Tafel equation, eqn. (4), for the steady-state cathodic hydrogen-evolution reaction with the experimental data gives the corrosion current density (i_{cor}) as well as the Tafel slope ($1/\alpha_H f$). Accordingly, from the experimental Tafel plots for HER on pure Pb, Pb–Ca–Sn and Pb–Sb–Se alloys in H_2SO_4 solution (3.67–10 M) with H_3PO_4 (0–40 g l^{-1}) and Sb(III) (0–10 mg l^{-1}) additives, the corrosion current densities have been calculated by back extrapolation of the Tafel plot to the corresponding steady-state corrosion potential (-968 ± 2 mV versus Hg/Hg_2SO_4 for [Sb(III)] = 0 and -965 ± 3 mV versus Hg/Hg_2SO_4 for [Sb(III)] = 1–10 mg l^{-1}). The dependence of the corrosion rates of lead and lead-alloy electrodes on the concentration of H_3PO_4 in H_2SO_4 at ≈ 25 °C, with and without Sb additive in the electrolyte, are shown in Figs. 1–4. The following conclusions can be drawn from the data.

(i) The hydrogen-evolution rate (corrosion rate) on pure Pb, Pb–Ca–Sn and Pb–Sb–Se alloys increases with increasing concentration on H_2SO_4.

(ii) H_3PO_4 additive decreases the rate of hydrogen evolution in all cases.

(iii) The decrease in the hydrogen-evolution rate caused by H_3PO_4 additive is largest at 20 g l^{-1} of H_3PO_4 concentration in solution.

(iv) In the presence of dissolved Sb(III) in solution, the hydrogen-evolution rate is enhanced in all cases.

*This notation is given according to IUPAC recommendations [12].

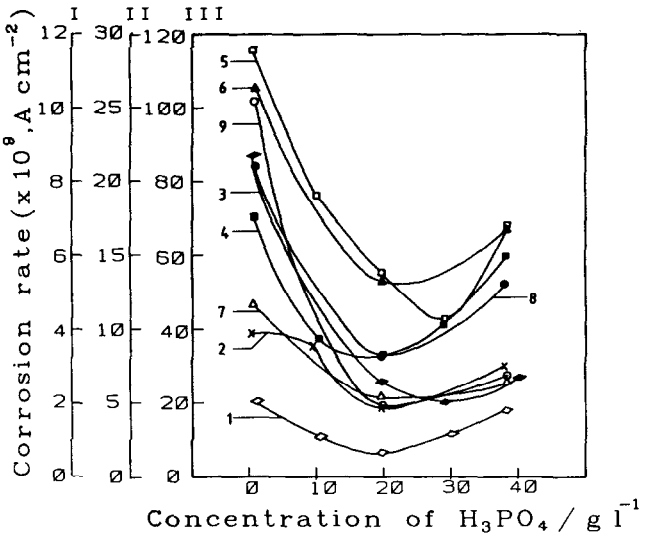

Fig. 1. Dependence of corrosion rate of Pb and Pb alloys on concentration of H_3PO_4 in H_2SO_4 (5.298 M) at 25±1 °C, and effect of Sb(III) additive to electrolyte: (1) Pb; [Sb(III)]: nil; (2) Pb–Ca–Sn; [Sb(III)]: nil; (3) Pb–Sb–Se; [Sb(III)]: nil; (4) Pb; [Sb(III)]: 1 mg l^{-1}; (5) Pb; [Sb(III)]: 10 mg l^{-1}; (6) Pb–Ca–Sn; [Sb(III)]: 1 mg l^{-1}; (7) Pb–Ca–Sn; [Sb(III)]: 10 mg l^{-1}; (8) Pb–Sb–Se; [Sb(III)]: 1 mg l^{-1}; (9) Pb–Sb–Se; [Sb(III)]: 10 mg l^{-1}. Ordinate scales are I (curves 1–4, 6), II (curves 5, 8) and III (curves 7, 9).

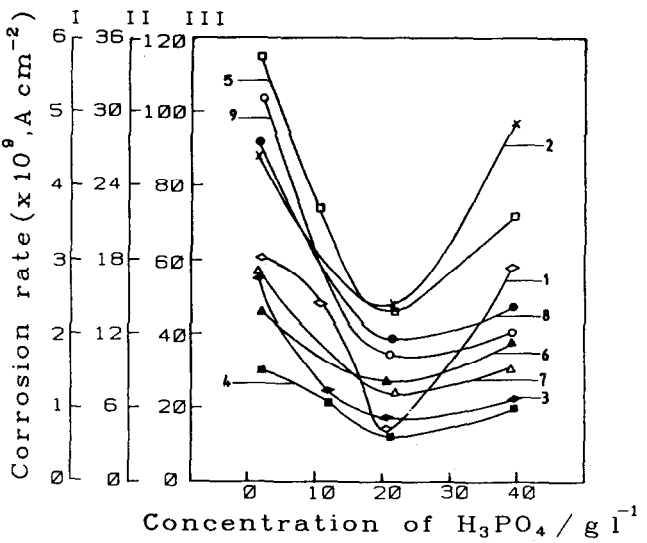

Fig. 2. Dependence of corrosion rate of Pb and Pb alloys on concentration of H_3PO_4 in H_2SO_4 (6.008 M) at 25±1 °C, and effect of Sb(III) additive to electrolyte: (1) Pb; [Sb(III)]: nil; (2) Pb–Ca–Sn; [Sb(III)]: nil; (3) Pb–Sb–Se; [Sb(III)]: nil; (4) Pb; [Sb(III)]: 1 mg l^{-1}; (5) Pb; [Sb(III)]: 10 mg l^{-1}; (6) Pb–Ca–Sn; [Sb(III)]: 1 mg l^{-1}; (7) Pb–Ca–Sn; [Sb(III)]: 10 mg l^{-1}; (8) Pb–Sb–Se; [Sb(III)]: 1 mg l^{-1}; (9) Pb–Sb–Se; [Sb(III)]: 10 mg l^{-1}. Ordinate scales are I (curves 1, 2), II (curves 3–6, 8), and III (curves 7, 9).

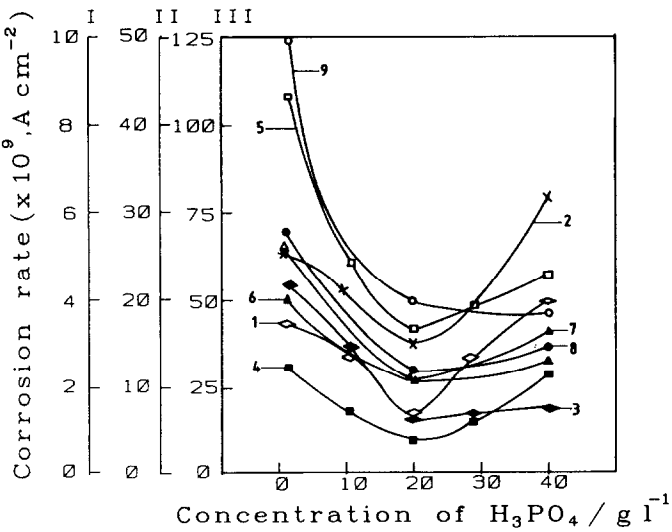

Fig. 3. Dependence of corrosion rate of Pb and Pb alloys on concentration of H_3PO_4 in H_2SO_4 (8.043 M) at 25±1 °C, and effect of Sb(III) additive to electrolyte: (1) Pb: [Sb(III)]: nil; (2) Pb–Ca–Sn; [Sb(III)]: nil; (3) Pb–Sb–Se; [Sb(III)]: nil; (4) Pb; [Sb(III)]: 1 mg l^{-1}; (5) Pb; [Sb(III)]: 10 mg l^{-1}; (6) Pb–Ca–Sn; [Sb(III)]: 1 mg l^{-1}; (7) Pb–Ca–Sn; [Sb(III)]: 10 mg l^{-1}; (8) Pb–Sb–Se; [Sb(III)]; 1 mg l^{-1}; (9) Pb–Sb–Se; [Sb(III)]: 10 mg l^{-1}. Ordinate scales are I (curves 1, 2), II (curves 3–6, 8), and III (curves 7, 9).

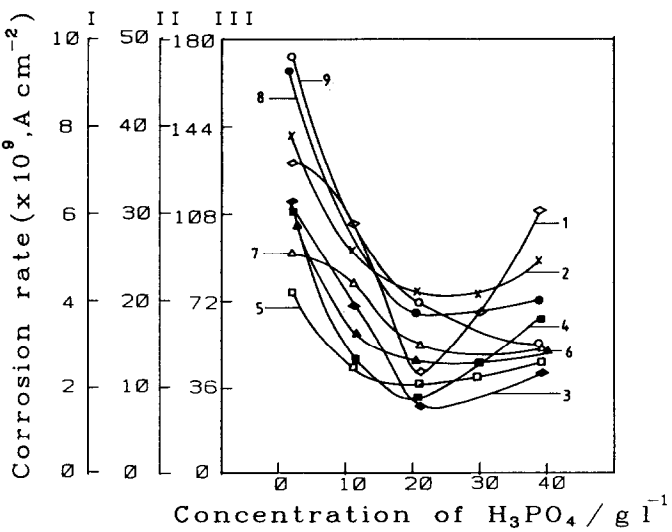

Fig. 4. Dependence of corrosion rate of Pb and Pb alloys on concentration of H_3PO_4 in H_2SO_4 (10.09 M) at 25±1 °C, and effect of Sb(III) additive to electrolyte: (1) Pb; [Sb(III)]: nil; (2)Pb–Ca–Sn; [Sb(III)]: nil; (3) Pb–Sb–Se; [Sb(III)]: nil; (4) Pb; [Sb(III)]: 1 mg l^{-1}; (5) Pb; [Sb(III)]: 10 mg l^{-1}; (6) Pb–Ca–Sn; [Sb(III)]: 1 mg l^{-1}; (7) Pb–Ca–Sn; [Sb(III)]: 10 mg l^{-1}; (8) Pb–Sb–Se; [Sb(III)]: 1 mg l^{-1}; (9) Pb–Sb–Se; [Sb(III)]: 10 mg l^{-1}. Ordinate scales are I (curves 1, 2), II (curves 3, 4, 6, 8), and III (curves 5, 7, 9).

(v) The increase in hydrogen-evolution rate due to dissolved antimony is diminished in the presence of H_3PO_4 additive as compared with the rate in the absence of this additive.

(iv) The Sb(III)-induced hydrogen-evolution rate is suppressed to a large extent at a concentration of 20 g l^{-1} H_3PO_4 additive in solution.

The above observations are explained in the light of the following model. On rewriting the current–potential equation for hydrogen evolution in terms of the standard rate constants of the partial reactions, we obtain:

$$I = nFA(1-\theta)\{K_H C_{H^+} \exp[-\alpha_H f(E-E^0_H)] - K_M C_M \exp[\beta_M f(E-E^0_M)]\} \quad (5)$$

In well-stirred solutions of high concentration, as in the present case, mass-transfer control is absent. Hence, $C_{H^+} = C^0_{H^+}$, $C_M = C^0_M$ and, therefore:

$$I = nFA(1-\theta)\{K_H C^0_{H^+} \exp[-\alpha_H f(E-E^0_H)] - K_M C^0_M \exp[\beta_M f(E-E^0_M)]\} \quad (6)$$

where $(1-\theta)$ is the fraction of the surface area available for the hydrogen-evolution reaction; θ is the degree of coverage of the surface by any adsorbed electro-inactive species. At the corrosion potential, $I=0$; and $E=E_{cor}$. Therefore, the above eqn. becomes:

$$0 = nFA(1-\theta)\{K_H C^0_{H^+} \exp[-\alpha_H f(E_{cor}-E^0_H)] - K_M C^0_M \exp[\beta_M f(E_{cor}-E^0_M)]\} \quad (7)$$

With each of the two terms on the right-hand side of the eqn. (7) being equal to I_{cor}, the following may be written:

$$I_{cor} = nFA(1-\theta)K_H C^0_{H^+} \exp[-\alpha_H f(E_{cor}-E^0_H)] \quad (8)$$

$$= nFA(1-\theta)K_M C^0_M \exp[\beta_M f(E_{cor}-E^0_M)] \quad (9)$$

Noting that $E^0_H = 0$:

$$I_{cor} = nFA(1-\theta)K_H C^0_{H^+} \exp[-\alpha_H f(E_{cor})] \quad (10)$$

The mechanism of action of H_3PO_4 additive in suppressing the rate of hydrogen evolution may be due its adsorption at the metal/solution interface. This suggestion is in agreement with that of other authors [9, 10, 13]. Then, θ in eqn. (10) may be identified with the fraction of the area covered by H_3PO_4 molecules (or $H_2PO_4^-$ ions). Thus,

$$I_{cor} \approx nFAK_H(C^0_{H_2SO_4} + C^0_{H_3PO_4})(1-\theta_{H_3PO_4}) \exp[-\alpha_H f(E_{cor})] \quad (11)$$

The following limiting cases may now be considered:

- case 1

$C^0_{H_3PO_4} \to \infty$; therefore, $\theta_{H_2PO_4^-} \approx \theta_{s(H_3PO_4)}$. $\theta_{s(H_3PO_4)}$ is the saturation value. Therefore,

$$I_{cor} \approx K'_H(C^0_{H_2SO_4} + C^0_{H_3PO_4}) \quad (12)$$

where:

$$K'_H = nFAK_H[1-\theta_{s(H_3PO_4)}] \exp(-\alpha_H f E_{cor}) \quad (13)$$

As indicated by eqn. (12), a linear increase in the hydrogen-evolution rate on lead and lead alloys is expected for an increase in the concentration of H_2SO_4 (in accordance with experiment) or H_3PO_4 or both. The expected trend with respect to $[H_3PO_4]$ is shown in curve (a) in Fig. 5.

- case 2

Considering the other extreme case where:

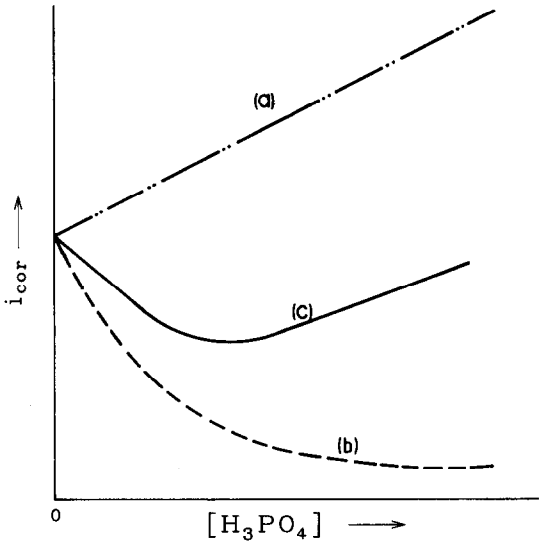

Fig. 5. Schematic dependence of i_{cor} on the concentration of H_3PO_4 additive in H_2SO_4 solution: (a) corresponding to the limiting case of $C^0_{H_3PO_4} \to \infty$, i.e., $\theta_{H_3PO_4} \approx \theta_{s(H_3PO_4)}$; (b) corresponding to the limiting case of $C^0_{H_3PO_4} \to 0$, i.e., $C^0_{H_3PO_4} \ll C^0_{H_2SO_4}$, and (c) net i_{cor} vs. $[H_3PO_4]$.

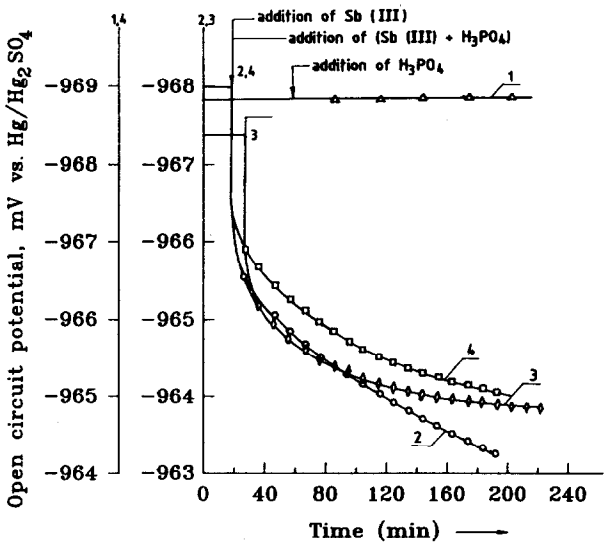

Fig. 6. Open-circuit potential–time transients of smooth Pb electrodes in H_2SO_4 (5.298 M) (curves 1–3), or in H_2SO_4 (5.298 M) + H_3PO_4 (40 g l^{-1}) mixed solution (curve 4), with additions of: (1) H_3PO_4 (40 g l^{-1}); (2) [Sb(III)] (1 mg l^{-1}); (3) [Sb(III)] (1 mg l^{-1}) + H_3PO_4 (40 g l^{-1}); (4) [Sb(III)] (1 mg l^{-1}). The additions 1–4 are made at the moments shown by arrows. Concentrations refer to the volume of the final solution.

$C^0_{H_3PO_4} \longrightarrow 0$; therefore, $C^0_{H_3PO_4} \ll C^0_{H_2SO_4}$

$$I_{cor} \approx K''_H(1-\theta_{H_3PO_4}) \tag{14}$$

where:

$$K''_H = nFAK_H C^0_{H_2SO_4} \exp[-\alpha_H f E_{cor}] \tag{15}$$

Equation (14) predicts an asymptotically decreasing value for I_{cor} with an increase in the H_3PO_4 concentration as shown in curve (b) in Fig. 5. Note, adsorption at an electrode/solution interface usually follows the Frumkin isotherm, i.e.:

$$\theta(1-\theta)^{-1} \exp(-2a\theta) = K_{ad} C^0 \tag{16}$$

where a is a constant (interaction parameter), and K_{ad} is the adsorption equilibrium constant. Hence θ varies asymptotically with C^0, the bulk concentration.

The general relationship is obtained by combining cases 1 and 2, which predicts a minimum in I_{cor} versus $[H_3PO_4]$. This is shown in curve (c) in Fig. 5. The minimum in the value of I_{cor} observed with an increase in $[H_3PO_4]$ additive in a solution of any given $[H_2SO_4]$ may be attributed to opposing trends: I_{cor} increases with the total acid concentration in solution, and I_{cor} decreases nonlinearly with $[H_3PO_4]$ concentration.

The occurrence of a minimum is common to all the electrodes studied, viz., Pb, Pb–Ca–Sn and Pb–Sb–Se. This is an indirect support to the above mechanistic explanation that does not depend on the nature of the lead alloy used. The most significant observation is that H_3PO_4 additive suppresses the Sb(III)-induced hydrogen-evolution rate on Pb and Pb alloys and may be analysed as follows.

The standard potential for SbO^+/Sb reaction ($E^0 = +0.21$ V) is more positive than that of the $Pb/PbSO_4$ reaction ($E^0 = -0.356$ V). Therefore, the deposition of elemental antimony on the lead surface is thermodynamically feasible and is likely to occur in H_2SO_4 solution. From the kinetics point of view, this reaction of galvanic deposition of antimony on a lead surface has been proved to occur under open-circuit conditions [14–17]. Since the corrosion of lead in de-aerated sulfuric acid involves only hydrogen depolarization, the rate of which is directly related to the kinetics of the HER on lead, it may be visualized that in the presence of Sb(III) in solution, the HER will occur not only on lead but also on antimony deposited on the lead surface. The overall rate of the HER and hence the corrosion rate of lead, are determined by the kinetics of the HER on lead, as well as on antimony. Since the overpotential for the HER on antimony is quite low [18–20] as compared with that on lead, the HER will occur at a significant rate on antimony and, thereby, will increase the rate of lead corrosion.

The mechanism of suppression of the Sb-induced hydrogen evolution on lead and lead alloys by H_3PO_4 is then to be attributed to a strong adsorption of H_3PO_4 on the antimony surface. Although direct evidence of this aspect may have to be obtained later on (for example, by contact angle measurements), the possibility of such an adsorption can be qualitatively judged from the open-circuit potential–time transients and galvanostatic cathodic polarization potential–time transients with and without H_3PO_4 additive, as shown in Figs. 6 and 7. The faster attainment of a steady-state and a cathodic shift in the steady-state potential observed above can only be due to the adsorption of H_3PO_4 on a Sb-contaminated surface.

An additional insight into the mechanism of action of H_3PO_4 additive in reducing the hydrogen-evolution rate on Pb, Pb–Ca–Sn and Pb–Sb–Se alloys in H_2SO_4 solution may be obtained by analysing the Tafel plots for the HER with respect to the kinetic

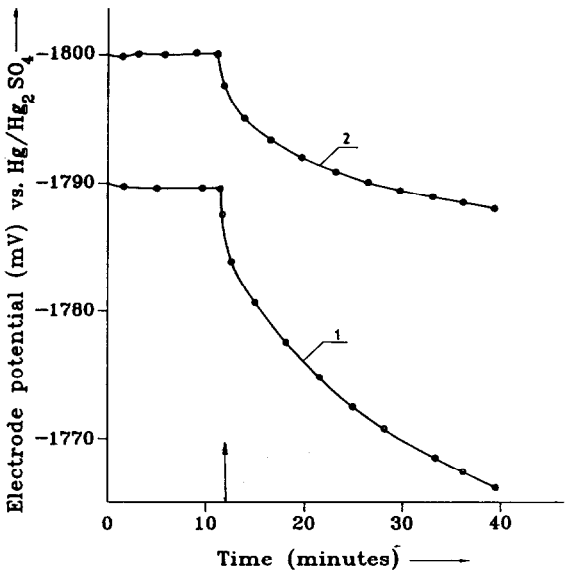

Fig. 7. Galvanostatic cathodic polarization transients for smooth Pb electrode on addition of [Sb(III)] (1 mg l^{-1}) to a solution of: (1) H_2SO_4 (5.298 M) and (2) H_2SO_4 (5.298 M) + H_3PO_4 (40 g l^{-1}). Current density: 10 mA cm^{-2}. Moments of addition of [Sb(III)] are shown by arrow. Concentrations refer to volume of the final solution.

parameters of the HER itself. As is well known from the Tafel theory, the exchange-current density for the HER is obtained by the extrapolation of the HER line to the reversible potential of the HER in the solution, namely −612 mV versus Hg/Hg_2SO_4. Note, this value of E_H^r is independent of acid concentration as may be readily seen from the Nernst equation for a cell that comprises the hydrogen-electrode reaction (with the partial pressure of hydrogen at 1 atm) and an Hg/Hg_2SO_4 electrode. Since the partial pressure of H_2 is close to 1 atm in all the present cases, this value is independent of acid concentration. The $i_{0,H}$ and Tafel slopes for the HER on Pb, Pb–Ca–Sn and Pb–Sb–Se alloys in H_2SO_4 solutions (3.67–10 M) with and without Sb(III) (0–10 mg l^{-1}) additive and H_3PO_4 (0–40 g l^{-1}) additive, as derived from the experimental Tafel lines, are in accord with the published data [21–26]. The mechanism of the HER that is valid in all these cases may therefore be taken as electron transfer to hydronium ions at the metal/solution interface as the rate-determining step and the recombination of hydrogen atoms on the surface as a subsequent fast step.

The dependence of $i_{0,H}$ on the concentration of H_3PO_4 with and without Sb(III) additive for different H_2SO_4 concentrations (3.67–10 M) is depicted in Figs. 8 to 11. Since the Tafel slope is unaltered, it gives an indication that the mechanism of action of H_3PO_4 in decreasing the corrosion rate of Pb, Pb–Ca–Sn and Pb–Sb–Se alloys, both in the presence or in the absence of Sb(III) in solution, is that of adsorption of H_3PO_4 at the interface and retardation of the kinetics on the HER at the interface without changing the Volmer mechanism of the HER itself [27].

The implication of the above novel finding that H_3PO_4 suppresses the Sb-induced hydrogen evolution on Pb, Pb–Ca–Sn and Pb–Sb–Se alloys is of considerable importance to the design of sealed lead/acid batteries. It must be established, however, that the

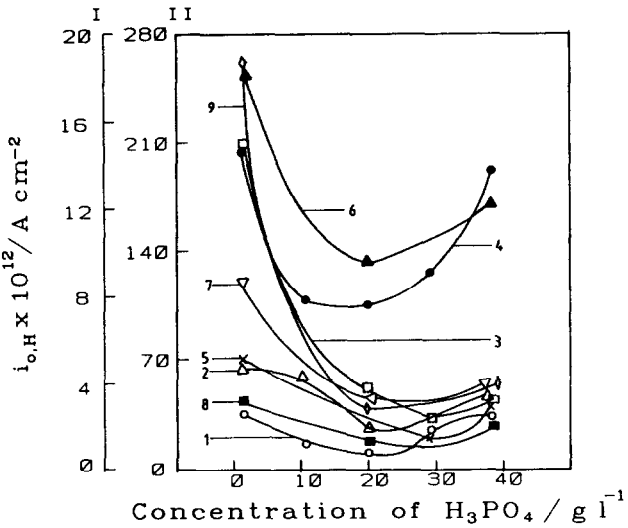

Fig. 8. Dependence of exchange-current density for HER on Pb and Pb alloys on concentration of H_3PO_4 in H_2SO_4 (5.298 M) at 25±1 °C, and effect of Sb(III) additive to electrolyte: (1) Pb; [Sb(III)]: nil; (2) Pb–Ca–Sn; [Sb(III)]: nil; (3) Pb–Sb–Se; [Sb(III)]: nil; (4) Pb; [Sb(III)]: 1 mg l^{-1}; (5) Pb; [Sb(III)]: 10 mg l^{-1}; (6) Pb–Ca–Sn; [Sb(III)]: 1 mg l^{-1}; (7) Pb–Ca–Sn; [Sb(III)]: 10 mg l^{-1}; (8) Pb–Sb–Se; [Sb(III)]: 1 mg l^{-1}; (9) Pb–Sb–Se; [Sb(III)]: 10 mg l^{-1}. Ordinate scales are I (curves 1–4, 6), and II (curves 5, 7–9).

H_3PO_4 additive does not affect adversely the kinetics of the desired Pb/Pb^{2+} reaction at the negative electrode.

The galvanostatic cathodic polarization data obtained by point-by-point measurement in the steady-state within the linear polarization domain for pure lead electrode in $PbSO_4$-saturated de-aerated H_2SO_4 solution, with and without H_3PO_4 additive, (Fig. 12) may be interpreted to give the desired information. For a quasi-reversible electrode such as $Pb/PbSO_4$ electrode, the general relationship between the overpotential $(E-E^r)$, faradaic current (I_{far}) and the mass-transfer-controlled concentrations C_O and C_R at the electrode surface is given by:

$$\frac{I_{far}}{I_0} = \frac{C_O}{C_O^0} \exp[-\alpha nf(E-E^r)] - \frac{C_R}{C_R^0} \exp[\beta nf(E-E^r)] \tag{17}$$

where I_0 is the exchange current, C_O^0 and C_R^0 are the concentrations of 'O' (oxidant) and 'R' (reductant) in the bulk (or beyond the diffusion layer), α and β are energy-transfer coefficients for the cathodic and anodic reactions, respectively, and $f=F/RT$. Linearization of eqn. (17) with the assumption that $(\alpha+\beta)=1$ gives:

$$\frac{I_{far}}{I_0} = \frac{C_O}{C_O^0} - \frac{C_R}{C_R^0} - nf(E-E_{cor}) \tag{18}$$

Equation (18) may be recast in the steady-state as:

$$I_{far}\left[\frac{1}{I_0} + \frac{1}{\tilde{I}_d} + \frac{1}{\tilde{I}_d}\right] = -nf(E-E_{cor}) \tag{19}$$

The term $1/\tilde{I}_d$ in eqn. (19) can be neglected compared with the other two terms due to the fact that $|\tilde{I}_d| \gg \tilde{I}_d$. Therefore,

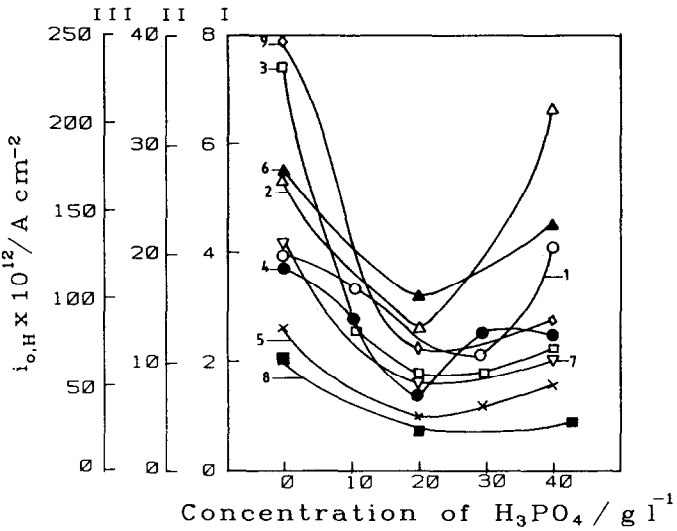

Fig. 9. Dependence of exchange-current density for HER on Pb and Pb alloys on concentration of H_3PO_4 in H_2SO_4 (6.008 M) at 25 ± 1 °C, and effect of Sb(III) additive to electrolyte: (1) Pb; [Sb(III)]: nil; (2) Pb–Ca–Sn; [Sb(III)]: nil; (3) Pb–Sb–Se; [Sb(III)]: nil; (4) Pb; [Sb(III)]: 1 mg l^{-1}; (5) Pb; [Sb(III)]: 10 mg l^{-1}; (6) Pb–Ca–Sn; [Sb(III)]: 1 mg l^{-1}; (7) Pb–Ca–Sn; [Sb(III)]: 10 mg l^{-1}; (8) Pb–Sb–Se; [Sb(III)]: 1 mg l^{-1}; (9) Pb–Sb–Se; [Sb(III)]: 10 mg l^{-1}. Ordinate scales are I (curves 1, 2), II (curves 3, 4, 6), and III (curves 5, 7–9).

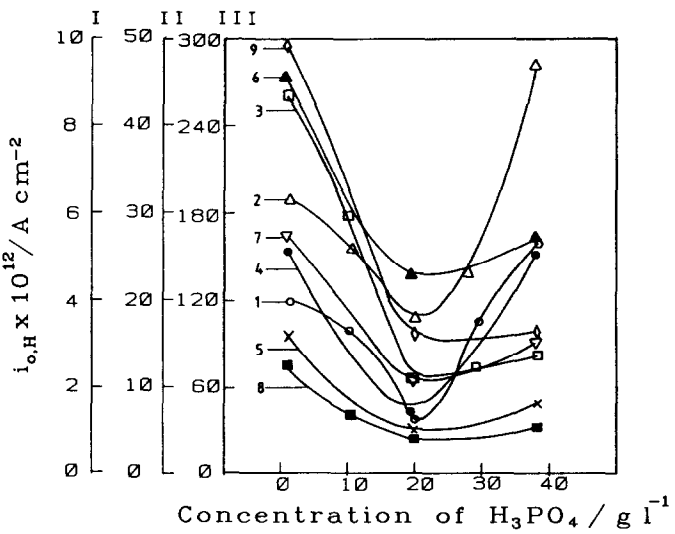

Fig. 10. Dependence of exchange-current density for HER on Pb and Pb alloys on concentration of H_3PO_4 in H_2SO_4 (8.043 M) at 25 ± 1 °C, and effect of Sb(III) additive to electrolyte: (1) Pb; [Sb(III)]: nil; (2) Pb–Ca–Sn; [Sb(III)]: nil; (3) Pb–Sb–Se; [Sb(III)]: nil; (4) Pb; [Sb(III)]: 1 mg l^{-1}; (5) Pb; [Sb(III)]: 10 mg l^{-1}; (6) Pb–Ca–Sn; [Sb(III)]: 1 mg l^{-1}; (7) Pb–Ca–Sn; [Sb(III)]: 10 mg l^{-1}; (8) Pb–Sb–Se; [Sb(III)]: 1mg l^{-1}; (9) Pb–Sb–Se; [Sb(III)]: 10 mg l^{-1}. Ordinate scales are I (curves 1, 2), II (curves 3, 4, 6), III (curves 5, 7–9).

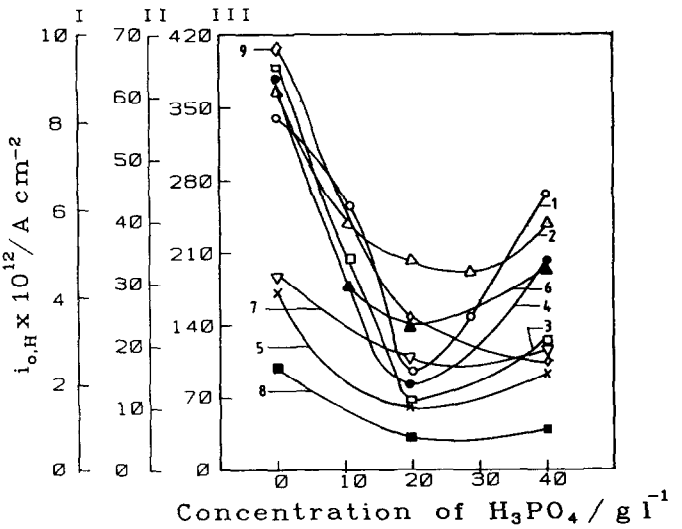

Fig. 11. Dependence of exchange-current density for HER on Pb and Pb alloys on concentration of H_3PO_4 in H_2SO_4 (10.09 M) at 25±1 °C, and effect of Sb(III) additive to electrolyte: (1) Pb; [Sb(III)]: nil; (2) Pb–Ca–Sn; [Sb(III)]: nil; (3) Pb–Sb–Se; [Sb(III)]: nil; (4) Pb; [Sb(III)]: 1 mg l^{-1}; (5) Pb; [Sb(III)]: 10 mg l^{-1}; (6) Pb–Ca–Sn; [Sb(III)]: 1 mg l^{-1}; (7) Pb–Ca–Sn; [Sb(III)]: 10 mg l^{-1}; (8) Pb–Sb–Se; [Sb(III)]: 1 mg l^{-1}; (9) Pb–Sb–Se; [Sb(III)]: 10 mg l^{-1}. Ordinate scales are I (curves 1, 2), II (curves 3, 4, 6), III (curves 5, 7–9).

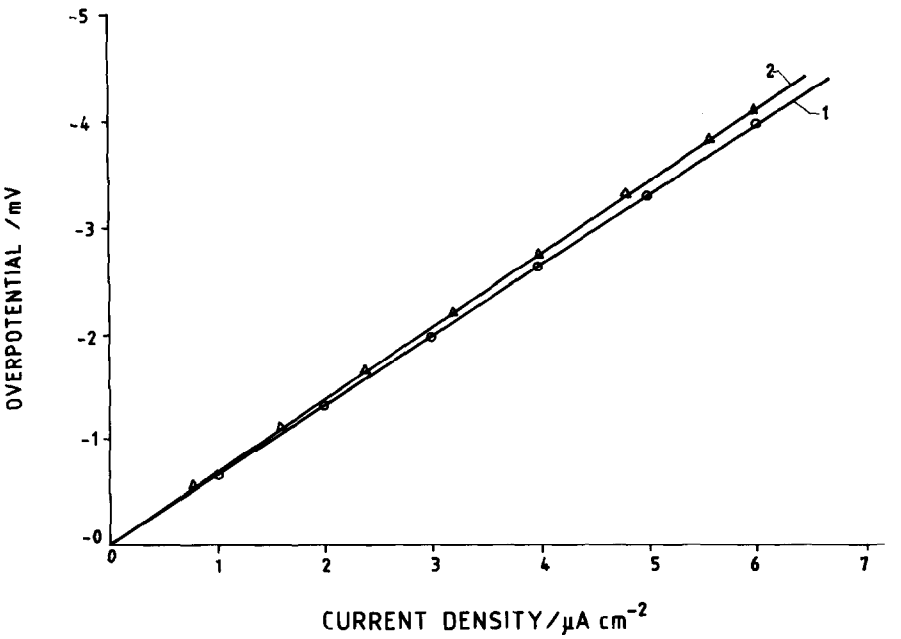

Fig. 12. Steady-state galvanostatic linear polarization for smooth Pb electrode in stirred solution saturated with $PbSO_4$: (1) H_2SO_4 (5.298 M), and (2) H_2SO_4 (5.298 M) + H_3PO_4 (40 g l^{-1}).

$$I_{far}\left[\frac{1}{I_0}+\frac{1}{\vec{I}_d}\right]=-nf(E-E_{cor}) \tag{20}$$

Substituting the values obtained from experiment for $\vec{I}_d$, I_{far} and $(E-E^r)$, I_0 for the Pb/Pb^{2+} was calculated. The exchange-current densities for the Pb/Pb^{2+} reaction on a lead electrode in sulfuric acid electrolyte, with and without phosphoric acid additive, are 2.15×10^{-5} and 2.34×10^{-5} A cm^{-2}, respectively. The data show that H_3PO_4 additive has practically no influence on the exchange current for the desired Pb^{2+}/Pb electrode reaction. The ameliorating effect from the presence of H_3PO_4 at about 20 g l^{-1} in the H_2SO_4 electrolyte used in the sealed lead/acid battery therefore appears to be highly attractive since the additive hinders the unwanted HER both in the presence and in the absence of Sb(III) in the electrolyte.

Conclusions

It is concluded that H_3PO_4 additive at about 20 g l^{-1} concentration in the H_2SO_4 electrolyte solution of a sealed lead/acid battery with a low-antimonial lead positive grid and an antimony-free negative grid is advantageous as it:

(i) decreases the rate of corrosion of lead and lead-alloys Pb–Ca–Sn and Pb–Sb–Se;

(ii) decreases the rate of open-circuit corrosion of lead and the lead-alloys Pb–Ca–Sn and Pb–Sb–Se;

(iii) decreases the deleterious effects of Sb(III), which tends to increase both the corrosion rate of, and also the hydrogen-evolution rate on, Pb, Pb–Ca–Sn and Pb–Sb–Se alloys, and

(iv) the rate of the desired electrode reaction (Pb/Pb^{2+}) is not adversely affected.

Acknowledgements

The author is indebted to late Professor S. Sathyanarayana of Indian Institute of Science, Bangalore, for suggesting the problem and for his invaluable guidance all through the course of this study. Thanks are also due to Dr A. Subrahmanyam, Head, Batteries Division, Mr B.L. Agrawal, Group Director, PSG, Mr P. Ramachandran, Deputy Director, ESA, ISAC, for permission to perform this work. The author is grateful to Director, ISAC, for permission to publish this paper.

List of symbols

$C^0_{H^+}$	concentration of H^+ in the bulk of the solution
$C^0_{H_2SO_4}$	concentration of H_2SO_4 in the bulk of the electrolyte
$C^0_{H_3PO_4}$	concentration of H_3PO_4 in the bulk of the electrolyte
C^0_M	concentration of the active sites for anodic dissolution of the metal in the bulk of the metal
C_O	concentration of oxidant at the electrode surface
C^0_O	concentration of oxidant in the bulk
C_R	concentration of reductant at the electrode surface
C^0_R	concentration of reductant in the bulk

E	potential of the working electrode versus Hg/Hg_2SO_4 reference electrode
E^0	standard electrode potential
E_{cor}	corrosion potential of the working electrode under a steady state
E^0_H	potential of the standard hydrogen electrode (SHE)
E^r	reversible potential
E^r_H	reversible potential for HER
E_+	potential of the Pb/PbO_2 electrode versus SHE
E_-	potential of the $Pb/PbSO_4$ electrode versus SHE
f	F/RT where, F is the Faraday constant, R the gas constant and T the absolute temperature
I_{cor}	corrosion current
i_{cor}	corrosion current density
$\vec{i}_d$	limiting current density for the forward reaction
$\overleftarrow{i}_d$	limiting current density for the reverse reaction
i_{far}	current density for the faradaic reaction
i_0	exchange-current density
$i_{0,H}$	exchange-current density for the hydrogen-evolution reaction
K_H	rate constant for hydrogen-evolution reaction at E^0_H
K_M	rate constant for metal dissolution reaction at E^0_M
n	number of electrons involved in the rate-determining step of the electrochemical reaction
α	cathodic energy-transfer coefficient
α_H	apparent energy-transfer coefficient for the cathodic hydrogen-evolution reaction
β	anodic energy-transfer coefficient
β_M	apparent energy-transfer coefficient for the anodic metal dissolution reaction
ξ	overpotential defined as $(E-E_{cor})$
θ_H	degree of coverage by adsorbed hydrogen
$\theta_{H_3PO_4}$	fraction of the area covered by adsorbed H_3PO_4 or $H_2PO_4^-$ species
$\theta_{s(H_3PO_4)}$	saturation value of $\theta_{H_3PO_4}$

References

1 R. Janakiraman, P.G. Balakrishnan, M. Devasahayam and S. Palanichamy, *Bull. Electrochem., 4* (1988) 563–564.
2 J. Szymborski and M.L. Eggers, *Proc. INTELEC'82 Conf.,* Institute of Electric and Electronic Engineers, New York, USA, p. 410.
3 D. Berndt and H. Franke, *Proc. INTELEC'87 Conf.,* Institute of Electric and Electronic Engineers, New York, USA, p. 115.
4 S. Laihonen, T. Laitinen, G. Sundholm and A. Yli-Pentti, *Electrochim. Acta, 35* (1990) 229.
5 A.F. Hollenkamp, *J. Power Sources, 36* (1991) 567–585.
6 S. Tudor, A. Wisstuch and S.H. Davang, *Electrochem. Technol., 3* (1965) 90; *4* (1966) 406; *5* (1967) 21.
7 Y. Song and J. Chen, *Dianchi, 21* (1991) 9.
8 O. Ikeda, C. Iwakura, H. Yoneyama and H. Tamura, *Technol. Rep. Osaka University, 36* (Oct.) (1986) 397–403.
9 J. Garche, H. Doring and K. Wiesener, *J. Power Sources, 33* (1991) 213.
10 G.A. Morris, P.J. Mitchell, N.A. Hampson and J.I. Dyson, in T. Keily and B.W. Baxter (eds.), *Power Sources 12,* Int. Power Sources Symposium Committee, Leatherhead, UK, 1989, pp. 61–75.
11 S. Venugopalan, *J. Power Sources, 46* (1993) 1–15.

12 K.E. Heusler, D. Landolt and S. Trasatti, *Electrochim. Acta, 35* (1990) 295–298.
13 M. Skyllas-Kazacos, *J. Power Sources, 13* (1984) 55–64.
14 J.L. Dawson, M.I. Gillibrand and J. Wilkinson, in D.H. Collins (ed.), *Power Sources 3*, Oriel Press, Newcastle upon Tyne, 1971, p. 1.
15 F. Burbank, A.C. Simon, E. Willihnganz, in P. Delahay and C.W. Tobias (eds.), *Advances in Electrochemistry and Electrochemical Engineering*, Vol. 8, New York, 1970, pp. 229–245.
16 H. Bode, *Lead–Acid Batteries*, Wiley, New York, 1977, pp. 238–242.
17 A.A. Jenkins, W.C. Maskell and F.L. Tye, *J. Power Sources, 19* (1987) 75–80.
18 I.A. Aguf and M.A. Dasoyan, *Sov. J. Appl. Chem., 32* (1959) 2022.
19 M. Barak, *Electrochemical Power Sources*, Peter Peregrinus, Stevenage, 1980, p. 200.
20 P. Ruetschi and R.T. Angstadt, *J. Electrochem. Soc., 105* (1958) 555.
21 K. Vijayamohanan, S. Sathyanarayana and S.N. Joshi, *J. Power Sources, 30* (1990) 169–175.
22 C.S.C. Bose and N.A. Hampson, *Bull. Electrochem., 4* (1988) 437–442.
23 A.N. Frumkin, in P. Delahay and C.W. Tobias (eds.), *Advances in Electrochemistry and Electrochemical Engineering*, Vol. 3, Interscience, New York, 1963, p. 296.
24 J. Thompson and S. Warrell, in J. Thompson (ed.), *Power Sources 9*, Academic Press, London, 1983, p. 97.
25 P. Ruetschi, J.B. Ockerman and R. Amlie, *J. Electrochem. Soc., 107* (1960) 325.
26 M.A. Dasoyan and A.I. Aguf, *Current theory of Lead/Acid Batteries*, Technicopy, Stonehouse, 1979, p. 320.
27 J.O'M. Bockris and A.K.N. Reddy, *Modern Electrochemistry*, Vol. 2, Plenum, New York, 1970, p. 1250.